

# Sequential nonabsorbing microwave single-photon detector

Ivan Iakoupov,<sup>\*</sup> Yuichiro Matsuzaki,<sup>†</sup> William J. Munro, and Shiro Saito

*NTT Basic Research Laboratories, NTT Corporation,  
3-1 Morinosato-Wakamiya, Atsugi, Kanagawa 243-0198, Japan*

(Dated: June 11, 2019)

We propose a nonabsorbing microwave single-photon detector that uses an artificial atom as a coherent interaction mediator between a traveling photon and a high- $Q$  resonator, fully exploiting the knowledge of the photon's arrival time. Our proposal can be implemented with the current level of technology and achieves distinguishability (probability of distinguishing between zero and one photon) in excess of 98% for realistic parameters. This is better than any of the similar detector proposals and realizations.

Efficiently detecting traveling microwave photons is an extremely challenging yet important task for future quantum technology. Currently, it is still not clear what is the best approach or whether there even *is* an approach that can be used in all situations. Out of the multitude of different proposals, we will restrict our attention here to the more versatile nonabsorbing detectors, so that detectors that absorb without reemitting or reemit the photon at a different frequency [1–9] are out of scope of this Letter. There is a number of recent proposals for the nonabsorbing microwave single-photon detectors [10–14] that can, in principle, be operated continuously, in the sense that the detector could be continuously interrogated for the presence of a photon. This way, both the presence of a photon and its arrival time could be obtained. The other type of the nonabsorbing detectors is the one that relies on knowledge of the photon's arrival time (or an arrival time window), and this is the approach taken in the recent experimental realizations [15, 16]. We will call this type of the detectors sequential, since their principle of operation usually consists of a sequence of different operations, where the simplest version involves two distinct steps: 1. interaction between the incident photon and the detector, 2. interrogation of the detector. For instance, in Refs. [15, 16], step 1 is the controlled-phase gate between the photon and an artificial atom [17]. Often, trying to perform step 2 simultaneously with step 1 results in the detector not working at all, since interrogation will prevent the interaction. The continuous-mode detectors have various approaches to make the interrogation during the interaction time be less detrimental [12–14].

The line between the continuous-mode and the sequential detectors is often blurred, however, as the continuous-mode detectors can also be operated sequentially where the sequence consists of “interrogation off” and “interrogation on”. This is the mode that is used for the calculation of one of the often used figures of merit for the single-photon detectors – the distinguishability (also known as “measurement fidelity”), which is the probability of correctly distinguishing between zero and one photon. Operationally, this is because the contribution of the signal due to an incident photon is finite, but the contribution of the (quantum and technical)

noise can always be increased by making the interrogation time longer. Therefore, the best distinguishability value is obtained when the interrogation starts from the arrival time of the incident photon and continues until some later time that is determined by the response of the detector. The equivalence of the distinguishability is important for the comparison of the sequential detector proposed in this Letter, its closest analogue among the continuous-mode detectors [13], and also the similar proposals [12, 14]. The reported distinguishabilities are in the range 70%-96%. Compared to those proposals, our proposed detector can no longer be operated in a continuous mode but achieves a better distinguishability.

We believe that our proposed detector could also be competitive against the existing experimental realizations of the sequential detectors [15, 16] where an artificial atom is used to store a state that is measured after an initial interaction with the incident photon, mediated by the resonator (see Fig. 1(a)). The proposed detector uses the resonator to store a state that is measured after an initial interaction with the incident photon, mediated by the artificial atom (see Fig. 1(b)). Thereby, our proposed detector reverses the roles of the artificial atom and the resonator. Technical details complicate the answer with respect to which approach is better (both give distinguishability  $\mathcal{F} = 100\%$  in the idealized limit), but it is usually easier to achieve long coherence time in resonators than in artificial atoms [19, 20]. Therefore, our proposed detector may be less susceptible to the errors due to the finite coherence time of the stored state.

The setup of our proposed detector is shown in Fig. 1(b). It consists of a three-level artificial atom and a resonator. The artificial atom is coupled both to an input transmission line and the resonator. From the input transmission line, a single photon is incident with a carrier frequency that is detuned from the  $|0\rangle \leftrightarrow |1\rangle$  transition by  $\delta_1$  (see Fig. 1(c)). The resonator is close in frequency to the transition  $|1\rangle \leftrightarrow |2\rangle$ , resulting in a coupling  $g$  with detuning  $\delta_2$ . The resonator frequency is assumed to be far detuned from the transition  $|0\rangle \leftrightarrow |1\rangle$  such that the coupling is negligible. The resonator is also assumed to not directly couple to the input transmission line, e.g., due to suppression of the coupling by a Purcell filter [21]

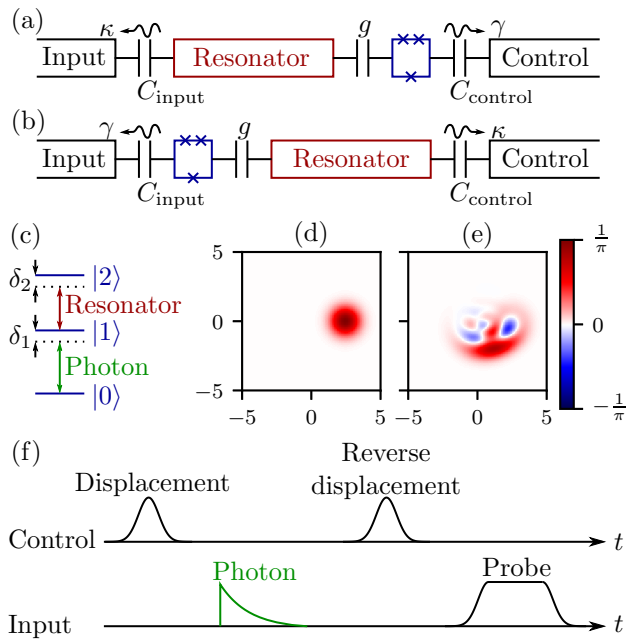


FIG. 1. (a) The usual microwave circuit QED setup. Here, with a persistent-current artificial atom [18] and capacitive couplings, but many other variations are possible. The coupling capacitance  $C_{\text{control}}$  is relatively small to prevent the artificial atom from decaying into the control transmission line (right). The coupling capacitance  $C_{\text{input}}$  is relatively large to facilitate the interaction of the fields in the input transmission line (left) with the resonator. The decay rates are indicated next to the respective capacitive coupling that gives rise to them ( $\gamma$  means both decay rates  $\gamma_{01}$  and  $\gamma_{12}$ ). (b) The setup employed for our proposed detector. The coupling capacitances are the same, but the places and the roles of the qubit and the resonator are reversed. (c) The level diagram of the artificial atom and indication of the system that the given transition is coupled to (either the incident photon or the resonator). (d) Wigner function of the initial coherent state of the resonator. The average photon number is  $\langle \hat{a}^\dagger \hat{a} \rangle = 3$  [13]. (e) Wigner function of the resonator state (reduced density matrix) after the interaction with an incident photon with bandwidth  $\gamma_c = 0.1\gamma_{01}$  for a time  $T_{\text{interact}} \approx 92/\gamma_{01}$ . The other parameters are:  $\kappa = 3.2 \cdot 10^{-5}\gamma_{01}$ ,  $\gamma_{11} = 3.2 \cdot 10^{-3}\gamma_{01}$ ,  $\gamma_{22} = 6.4 \cdot 10^{-3}\gamma_{01}$ ,  $\gamma_{12} = 0.1\gamma_{01}$ ,  $\delta_1 \approx -1.380\gamma_{01}$ ,  $\delta_2 \approx -96.89\gamma_{01}$ ,  $g \approx 7\gamma_{01}$ .  $T_{\text{interact}}$ ,  $\delta_1$  and  $\delta_2$  were chosen to minimize the error probability  $P_{E,M}$ , giving  $P_{E,M} \approx P_{E,\text{opt}} \approx 2.2\%$ . (f) The proposed detection sequence for the setup in (b). The single-photon field is green and classical drives (displacements and probe) are black. They are incident from the two different transmission lines (“Control” and “Input”).

at the resonator frequency attached to the input transmission line (left in Fig. 1(b), not shown). Depending on the bandwidth, the same or a different Purcell filter could also suppress the decay from the state  $|2\rangle$  of the artificial atom, resulting in a small decay rate  $\gamma_{12} = 0.1\gamma_{01}$  that was assumed in Ref. [13]. We keep the same value for

an easier comparison. The resonator is also coupled to a control transmission line with decay rate  $\kappa$ , making it possible to perform displacements of the resonator field.

The setup described above is very similar to the setup of Ref. [13], but with important differences, as described below. The Hamiltonian for our setup in the interaction picture with the rotating wave approximation made is

$$H = \hbar\delta_1\hat{\sigma}_{11} + \hbar(\delta_1 + \delta_2)\hat{\sigma}_{22} - i\hbar g(\hat{a}\hat{\sigma}_{21} - \hat{a}^\dagger\hat{\sigma}_{12}), \quad (1)$$

where  $\hat{\sigma}_{\mu\nu} = |\mu\rangle\langle\nu|$  are the atomic operators, and  $\hat{a}$  is the annihilation operator of the resonator. Compared to the Hamiltonian of Ref. [13], the above Hamiltonian does not have the term  $-i\hbar E(\hat{a} - \hat{a}^\dagger)$  that describes the always-on drive of the resonator. This is because in our proposal, the Rabi frequency  $E$  is set to zero during the entire detection sequence, except for the displacements that assume a large enough  $E$  for the displacements to happen in a time much shorter than any other time scale.

The incident photon that arrives from the input transmission line is modeled by a source resonator with decay rate  $\gamma_c$  [11–14], setting the mode shape of the photon to be a decaying exponential in time. The corresponding master equation is [13]

$$\begin{aligned} \dot{\rho} = \mathcal{L}\rho = & -\frac{i}{\hbar}[H, \rho] + \gamma_c\mathcal{D}[\hat{c}]\rho + \gamma_{01}\mathcal{D}[\hat{\sigma}_{01}]\rho \\ & + \gamma_{12}\mathcal{D}[\hat{\sigma}_{12}]\rho + \kappa\mathcal{D}[\hat{a}]\rho \\ & + \sqrt{\gamma_c\gamma_{01}}([\hat{c}\rho, \hat{\sigma}_{10}] + [\hat{\sigma}_{01}, \rho\hat{c}^\dagger]), \end{aligned} \quad (2)$$

where  $\mathcal{D}[\hat{r}]\rho = \frac{1}{2}(2\hat{r}\rho\hat{r}^\dagger - \hat{r}^\dagger\hat{r}\rho - \rho\hat{r}^\dagger\hat{r})$ ,  $\hat{c}$  is the annihilation operator of the source resonator, and the terms proportional to  $\sqrt{\gamma_c\gamma_{01}}$  describe the coupling of the source resonator to the artificial atom using the cascaded systems formalism [22, 23]. Setting  $\kappa$  to be much smaller than in Ref. [13] (which used  $\kappa = 0.037\gamma_{01}$ ) is the key difference of our proposal. Ideally,  $\kappa \rightarrow 0$  can be taken, corresponding to the limit of  $\kappa$  being negligible on the time scales of the detection sequence. Such a choice of  $\kappa$  prevents the continuous-mode operation (possible in the proposal of Ref. [13]), because the resonator state cannot be probed directly. Instead, we propose a detection sequence (Fig. 1(f)) whose final step is to probe the artificial atom to gain the information about the resonator state. Before we go in the details about this procedure, we can explain the high distinguishability of the detector by considering the distinguishability of the resonator states for the cases with and without an incident photon.

The detection sequence starts by initializing the artificial atom in state  $|0\rangle$  and the resonator in a coherent state. The latter could be accomplished by initializing in a vacuum state and displacing it. We choose the average photon number  $\langle \hat{a}^\dagger \hat{a} \rangle = 3$  [13], resulting in the coherent state of Fig. 1(d). At this point, an incident photon will change the state into the one shown in Fig. 1(e), otherwise the resonator state stays the same. We use two different distinguishability measures for the states.

The first one is the distinguishability  $\mathcal{F}_{\text{opt}}$  that gives the probability of correctly distinguishing between states in Figs. 1(d) and (e) using an optimal measurement and assuming a 50/50 probability of the two states. It can be written  $\mathcal{F}_{\text{opt}} = 1 - P_{\text{E,opt}}$ , where [24]

$$P_{\text{E,opt}} = \frac{1}{2} - \frac{1}{4} \|\rho_0 - \rho_1\|_{\text{tr}}, \quad (3)$$

with  $\|\rho_0 - \rho_1\|_{\text{tr}}$  being the trace norm of the difference of the reduced density matrices of the resonator,  $\rho_0$  and  $\rho_1$ , that correspond to Figs. 1(d) and (e), respectively. The second state distinguishability measure uses two measurement operators:  $M_0 = |\alpha\rangle\langle\alpha|$  and  $M_1 = I - M_0$ , where  $|\alpha\rangle$  is the coherent state in Fig. 1(d), and  $I$  is the identity operator. Then the distinguishability is  $\mathcal{F}_M = 1 - P_{\text{E},M}$ , where [25]

$$P_{\text{E},M} = \frac{1}{2} \text{tr}(\rho_0 M_1) + \frac{1}{2} \text{tr}(\rho_1 M_0), \quad (4)$$

again assuming a 50/50 probability of the two states  $\rho_0$  and  $\rho_1$ . This second state distinguishability measure is an idealization of the more realistic measurement procedure that we will discuss later.

To model the pure dephasing of the artificial atom, we add the terms  $\gamma_{11}\mathcal{D}[\hat{\sigma}_{11}]\rho$  and  $\gamma_{22}\mathcal{D}[\hat{\sigma}_{22}]\rho$  to the master equation (2) and set  $\gamma_{22} = 2\gamma_{11}$  to account for the larger dephasing rate of the higher energy levels [26]. Assuming the decay rate  $\gamma_{01} = 2\pi \cdot 10$  MHz and the pure dephasing time  $T_{\phi,\text{AA}} = 10$   $\mu\text{s}$  for the artificial atom, we have  $\gamma_{11}/\gamma_{01} = 2/(T_{\phi,\text{AA}}\gamma_{01}) \approx 3.2 \cdot 10^{-3}$  and  $\gamma_{22}/\gamma_{01} \approx 6.4 \cdot 10^{-3}$ . For the resonator, we assume  $T_{1,\text{R}} = 500$   $\mu\text{s}$  [27], giving  $\kappa/\gamma_{01} = 1/(T_{1,\text{R}}\gamma_{01}) \approx 3.2 \cdot 10^{-5}$ . The other imperfections in the model are the non-zero ratio  $\gamma_c/\gamma_{01}$  and the imperfect dispersive interaction. The latter depends on how close the Hamiltonian (1) is to the perfect dispersive Hamiltonian

$$H_{\text{disp}} = \hbar\delta_1\hat{\sigma}_{11} - \hbar\chi\hat{\sigma}_{11}\hat{a}^\dagger\hat{a}, \quad (5)$$

where  $\chi = g^2/(\delta_1 + \delta_2)$ . We choose  $g = 7\gamma_{01} = 2\pi \cdot 70$  MHz [27].

In Fig. 2, we vary  $\gamma_c$  and plot  $P_{\text{E},M}$  for optimal  $\delta_1$  and  $\delta_2$  using both Hamiltonians  $H$  and  $H_{\text{disp}}$ . For those parameters,  $P_{\text{E,opt}} \approx P_{\text{E},M}$ , which would have lead to completely overlapping curves in Fig. 2. This is not always the case: if we used exactly the same parameters as in Ref. [13] except setting  $\kappa = 0$  ( $\gamma_c/\gamma_{01} = 0.1$ ,  $\gamma_{11} = \gamma_{22} = 0$ ,  $\delta_1 = -0.8\gamma_{01}$ ,  $\delta_2 = -18\gamma_{01}$ ,  $g = 2.45\gamma_{01}$ ) then  $P_{\text{E},M} \approx 6.7\%$  and  $P_{\text{E,opt}} \approx 4.6\%$ .

The solid red curve in Fig. 2 shows our results with the most complete model of the imperfections that uses the Hamiltonian (1) with non-zero  $\kappa$ ,  $\gamma_{11}$ , and  $\gamma_{22}$ . The states in Figs. 1(d) and (e) correspond to  $\gamma_c/\gamma_{01} = 0.1$  on this curve. The dashed green curve only differs from the solid red one in setting  $\kappa = 0$ . The dash-dotted blue curve represents the almost ideal case with  $\kappa = \gamma_{11} = \gamma_{22} = 0$

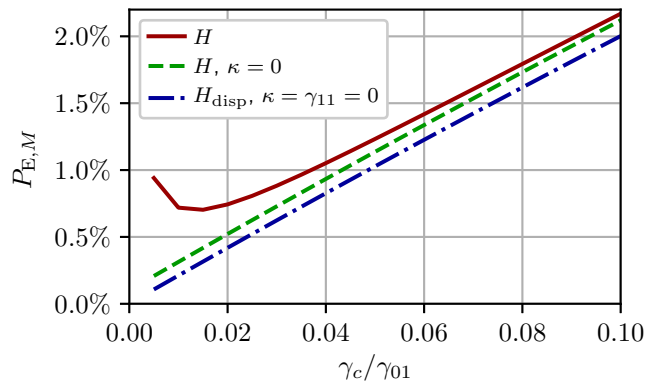


FIG. 2. Error probabilities  $P_{\text{E},M}$  as a function of the input photon bandwidth  $\gamma_c$ . The interaction time  $T_{\text{interact}}$  is varied such that  $T_{\text{interact}} \leq 10/\gamma_c$  with the smallest  $P_{\text{E},M}$  is chosen. The legend indicates the used Hamiltonian and whether some decay rates are set to zero. Unless indicated by  $\kappa = 0$ , we set  $\kappa = 3.2 \cdot 10^{-5}\gamma_{01}$ . Indication  $\gamma_{11} = 0$  also implies  $\gamma_{22} = 0$ , otherwise we set  $\gamma_{11} = 3.2 \cdot 10^{-3}\gamma_{01}$  and  $\gamma_{22} = 6.4 \cdot 10^{-3}\gamma_{01}$ . Common parameters are:  $\gamma_{12} = 0.1\gamma_{01}$ ,  $g = 7\gamma_{01}$ . For each value of  $\gamma_c/\gamma_{01}$ ,  $\delta_1$  and  $\delta_2$  were chosen to minimize  $P_{\text{E},M}$ .

and uses the Hamiltonian (5) so that it is only limited by the non-zero ratio  $\gamma_c/\gamma_{01}$ , achieving  $\mathcal{F}_M = 100\%$  for  $\gamma_c/\gamma_{01} \rightarrow 0$ . Comparison of these curves illustrates the different effect of the imperfections of the artificial atom and the resonator. The imperfections of the artificial atom add a constant term to  $P_{\text{E},M}$ , since the artificial atom only acts as a mediator of the interaction and effectively stores every part of the incident photon only for a limited time. The non-zero  $\kappa$  of the resonator, on the other hand, gives a larger error with smaller  $\gamma_c/\gamma_{01}$ , since the state has to be stored in the resonator for a longer time.

A realization of the measurement used for  $\mathcal{F}_M$  starts with an unconditional displacement of the states in Figs. 1(d) and (e) such that the coherent state in Fig. 1(d) becomes the vacuum state  $|\text{vac}\rangle$ , and the ideal measurement operators become  $M_0 = |\text{vac}\rangle\langle\text{vac}|$  and  $M_1 = I - M_0$ . An implementation of these measurement operators can be done by driving the artificial atom by a continuous wave field with a frequency close to the transition  $|0\rangle \leftrightarrow |1\rangle$  from the input transmission line and doing homodyne detection of the reflected field. The idea is that the dispersive interaction of the artificial atom with the resonator (see Eq. (5)) shifts the frequency of the transition  $|0\rangle \leftrightarrow |1\rangle$  only if the resonator is in a state different from vacuum. This conditional frequency shift of the transition  $|0\rangle \leftrightarrow |1\rangle$  gives a conditional phase shift of the reflected probe field applied at a fixed frequency. The complete detection sequence is summarized in Fig. 1(f).

The probing of the artificial atom is described by an additional Hamiltonian term  $\hbar\Omega(\hat{\sigma}_{01} + \hat{\sigma}_{10})$ , where  $\Omega$  is the Rabi frequency of the continuous wave drive, and

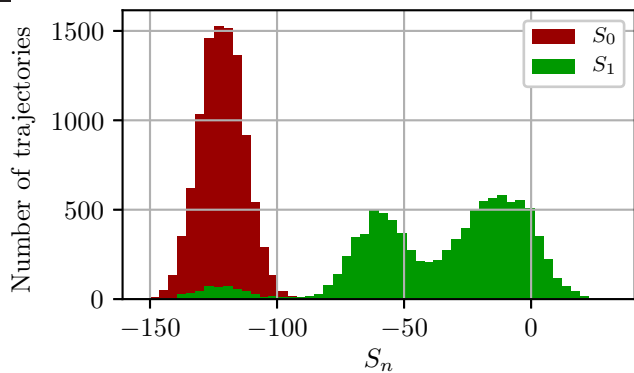


FIG. 3. Histogram of the filtered integrated homodyne currents,  $S_0$  and  $S_1$ , that correspond to the case without and with an incident photon, respectively. The parameters correspond to  $\gamma_c/\gamma_{01} = 0.1$  on the solid red curve in Fig. 2 ( $\kappa = 3.2 \cdot 10^{-5}\gamma_{01}$ ,  $\gamma_{11} = 3.2 \cdot 10^{-3}\gamma_{01}$ ,  $\gamma_{22} = 6.4 \cdot 10^{-3}\gamma_{01}$ ,  $\gamma_{12} = 0.1\gamma_{01}$ ,  $g = 7\gamma_{01}$ ,  $\delta_1 \approx -1.380\gamma_{01}$ ,  $\delta_2 \approx -96.89\gamma_{01}$ ,  $T_{\text{interact}} = 92/\gamma_{01}$ ). The parameters for probing of the artificial atom are:  $\delta_1 = 0.1\gamma_{01}$ ,  $\phi = \pi/2$ ,  $\Omega = 0.2\gamma_{01}$ ,  $T_{\text{probe}} = 500/\gamma_{01}$ . The total number of the trajectories is  $N_{\text{tot}} = 10^4$ . The resulting error probability is  $P_{E,M,\text{real}} \approx 2.4\%$ .

using the stochastic master equation [11–14]

$$d\rho = \mathcal{L}\rho dt + dW(t)\mathcal{H}[\hat{O}]\rho, \quad (6)$$

where  $\mathcal{H}[\hat{r}]\rho = \hat{r}\rho + \rho\hat{r}^\dagger - \text{tr}(\hat{r}\rho + \rho\hat{r}^\dagger)\rho$ ,  $\hat{O} = e^{-i\phi}\sqrt{\gamma_{01}}\hat{\sigma}_{01}$ , with  $dW(t)$  being a Wiener process. The corresponding homodyne current is

$$I_n(t) = \langle \hat{O} + \hat{O}^\dagger \rangle + dW(t)/dt, \quad (7)$$

where the subscript  $n$  can be 1 or 0 – indicating whether a photon was incident or not, respectively. To filter this homodyne current, we define  $\bar{I}_n(t) = \langle \hat{O} + \hat{O}^\dagger \rangle$  where the expectation value uses the density matrix evolved with the deterministic master equation (2). The filtered integrated homodyne current is then

$$S_n = \int_0^{T_{\text{probe}}} I_n(t)h(t)dt, \quad (8)$$

where the filter is  $h(t) = |\bar{I}_0(t) - \bar{I}_1(t)|$ . We generate  $N_{\text{tot}} = 10^4$  trajectories for each of the cases  $n = 0$  and  $n = 1$ , resulting in the integrals  $S_{n,j}$ , where  $j$  is the trajectory index. The distinguishability is then  $\mathcal{F}_{M,\text{real}} = 1 - P_{E,M,\text{real}}$ , where (for a 50/50 probability of the two states)

$$P_{E,M,\text{real}} = \frac{1}{2} \frac{N_{S_{0,j} > S_{\text{thr}}}}{N_{\text{tot}}} + \frac{1}{2} \frac{N_{S_{1,j} < S_{\text{thr}}}}{N_{\text{tot}}}, \quad (9)$$

with  $N_{S_{0,j} > S_{\text{thr}}}$  ( $N_{S_{1,j} < S_{\text{thr}}}$ ) being the number of the integrals  $S_{0,j}$  ( $S_{1,j}$ ) that are above (below) the threshold  $S_{\text{thr}}$ . The threshold  $S_{\text{thr}}$  is chosen such that  $P_{E,M,\text{real}}$  is

minimized. This definition assumes that, on average, the integrals  $S_{0,j}$  are smaller than the integrals  $S_{1,j}$ . It is the case in Fig. 3 which corresponds to  $\gamma_c/\gamma_{01} = 0.1$  on the solid red curve in Fig. 2. The resulting error probability is  $P_{E,M,\text{real}} \approx 2.4\%$  that is slightly larger than  $P_{E,M} \approx 2.2\%$  for the same interaction parameters. It might be possible to optimize the probing parameters (see caption of Fig. 3) further to make the difference smaller.

The distinguishability of our sequential detector proposal compares favorably against the distinguishability reported for the continuous-mode detector proposals [12–14], even if they use several artificial atoms. As shown in Fig. 2, we report distinguishabilities  $\mathcal{F} = 98\%$  and above for  $\gamma_c/\gamma_{01} \leq 0.1$ , which are better than the reported distinguishabilities in Refs. [12–14] (70%–96%). In the other proposals, the artificial atom decay rates may have a range of values [12], or the collective effects may make the single artificial atom rate less relevant than the decay rate of the entire ensemble [14]. In the former case [12],  $\mathcal{F} = 90\%$  is reported for 8 artificial atoms where  $\gamma_c/\gamma_{01}$  varies between 0.5 and 0.1 for the different artificial atoms. In the latter case [14],  $\gamma_c/\gamma_B = 0.1$  is used, where  $\gamma_B$  is the decay rate of the bright state of the ensemble, resulting in  $\mathcal{F} = 96\%$  for 4 artificial atoms and 1 resonator. The proposal of Ref. [13] uses  $\gamma_c/\gamma_{01} = 0.1$  and reports  $\mathcal{F} = 90\%$  for 2 artificial atoms and 2 resonators. Thus, our proposed detector achieves higher distinguishability with less experimental complexity (1 artificial atom and 1 resonator).

In conclusion, we propose a nonabsorbing microwave single-photon detector with a larger distinguishability than in the similar proposals [12–14]. We accomplish this by completely removing the option of the continuous-mode operation (without the knowledge of the photon’s arrival time) in the proposal of Ref. [13] and introducing a new detection sequence. Our proposal is different from the previous sequential setups [15, 16], as the roles of the artificial atom and the resonator are reversed such that the resonator is used as storage, instead of the artificial atom. This difference may make our proposal more attractive due to often better coherence properties of the resonators compared to the artificial atoms.

We thank I. Mahboob and R. Budoyo for useful comments. This work was supported by CREST(JPMJCR1774), JST.

\* iakoupov.ivan.mh@hco.ntt.co.jp

† Current address: Nanoelectronics Research Institute, National Institute of Advanced Industrial Science and Technology (AIST), 1-1-1 Umezono, Tsukuba, Ibaraki 305-8568, Japan

[1] G. Romero, J. J. García-Ripoll, and E. Solano, Phys. Rev. Lett. **102**, 173602 (2009).  
[2] Y.-F. Chen, D. Hover, S. Sendelbach, L. Maurer, S. T.

- Merkel, E. J. Pritchett, F. K. Wilhelm, and R. McDermott, *Phys. Rev. Lett.* **107**, 217401 (2011).
- [3] K. Koshino, K. Inomata, T. Yamamoto, and Y. Nakamura, *Phys. Rev. Lett.* **111**, 153601 (2013).
- [4] K. Koshino, K. Inomata, Z. Lin, Y. Nakamura, and T. Yamamoto, *Phys. Rev. A* **91**, 043805 (2015).
- [5] K. Inomata, Z. Lin, K. Koshino, W. D. Oliver, J.-S. Tsai, T. Yamamoto, and Y. Nakamura, *Nature Communications* **7**, 12303 (2016).
- [6] O. Kyriienko and A. S. Sørensen, *Phys. Rev. Lett.* **117**, 140503 (2016).
- [7] G. Oelsner, C. K. Andersen, M. Reháč, M. Schmelz, S. Anders, M. Grajcar, U. Hübner, K. Mølmer, and E. Il'ichev, *Phys. Rev. Applied* **7**, 014012 (2017).
- [8] J. Leppäkangas, M. Marthaler, D. Hazra, S. Jebari, R. Albert, F. Blanchet, G. Johansson, and M. Hofheinz, *Phys. Rev. A* **97**, 013855 (2018).
- [9] R. Lescanne, S. Delglise, E. Albertinale, U. Rglade, T. Capelle, E. Ivanov, T. Jacqmin, Z. Leghtas, and E. Flurin, (2019), arXiv:1902.05102.
- [10] F. Helmer, M. Mariantoni, E. Solano, and F. Marquardt, *Phys. Rev. A* **79**, 052115 (2009).
- [11] B. Fan, A. F. Kockum, J. Combes, G. Johansson, I.-c. Hoi, C. M. Wilson, P. Delsing, G. J. Milburn, and T. M. Stace, *Phys. Rev. Lett.* **110**, 053601 (2013).
- [12] S. R. Sathyamoorthy, L. Tornberg, A. F. Kockum, B. Q. Baragiola, J. Combes, C. M. Wilson, T. M. Stace, and G. Johansson, *Phys. Rev. Lett.* **112**, 093601 (2014).
- [13] B. Fan, G. Johansson, J. Combes, G. J. Milburn, and T. M. Stace, *Phys. Rev. B* **90**, 035132 (2014).
- [14] B. Royer, A. L. Grimsmo, A. Choquette-Poitevin, and A. Blais, *Phys. Rev. Lett.* **120**, 203602 (2018).
- [15] S. Kono, K. Koshino, Y. Tabuchi, A. Noguchi, and Y. Nakamura, *Nature Physics* **14**, 546 (2018).
- [16] J.-C. Besse, S. Gasparinetti, M. C. Collodo, T. Walter, P. Kurpiers, M. Pechal, C. Eichler, and A. Wallraff, *Phys. Rev. X* **8**, 021003 (2018).
- [17] L.-M. Duan and H. J. Kimble, *Phys. Rev. Lett.* **92**, 127902 (2004).
- [18] T. P. Orlando, J. E. Mooij, L. Tian, C. H. van der Wal, L. S. Levitov, S. Lloyd, and J. J. Mazo, *Phys. Rev. B* **60**, 15398 (1999).
- [19] M. Reagor, W. Pfaff, C. Axline, R. W. Heeres, N. Ofek, K. Sliwa, E. Holland, C. Wang, J. Blumoff, K. Chou, M. J. Hatridge, L. Frunzio, M. H. Devoret, L. Jiang, and R. J. Schoelkopf, *Phys. Rev. B* **94**, 014506 (2016).
- [20] C. Wang, Y. Y. Gao, P. Reinhold, R. W. Heeres, N. Ofek, K. Chou, C. Axline, M. Reagor, J. Blumoff, K. M. Sliwa, L. Frunzio, S. M. Girvin, L. Jiang, M. Mirrahimi, M. H. Devoret, and R. J. Schoelkopf, *Science* **352**, 1087 (2016).
- [21] M. D. Reed, B. R. Johnson, A. A. Houck, L. DiCarlo, J. M. Chow, D. I. Schuster, L. Frunzio, and R. J. Schoelkopf, *Applied Physics Letters* **96**, 203110 (2010).
- [22] C. W. Gardiner, *Phys. Rev. Lett.* **70**, 2269 (1993).
- [23] H. J. Carmichael, *Phys. Rev. Lett.* **70**, 2273 (1993).
- [24] C. A. Fuchs and J. van de Graaf, *IEEE Transactions on Information Theory* **45**, 1216 (1999).
- [25] J. M. Geremia, *Phys. Rev. A* **70**, 062303 (2004).
- [26] M. J. Peterer, S. J. Bader, X. Jin, F. Yan, A. Kamal, T. J. Gudmundsen, P. J. Leek, T. P. Orlando, W. D. Oliver, and S. Gustavsson, *Phys. Rev. Lett.* **114**, 010501 (2015).
- [27] C. J. Axline, L. D. Burkhardt, W. Pfaff, M. Zhang, K. Chou, P. Campagne-Ibarcq, P. Reinhold, L. Frunzio, S. M. Girvin, L. Jiang, M. H. Devoret, and R. J. Schoelkopf, *Nature Physics* **14**, 705 (2018).